Report

Cell Reports

The Hippo Pathway Effector TAZ Regulates Ferroptosis in Renal Cell Carcinoma

Graphical Abstract

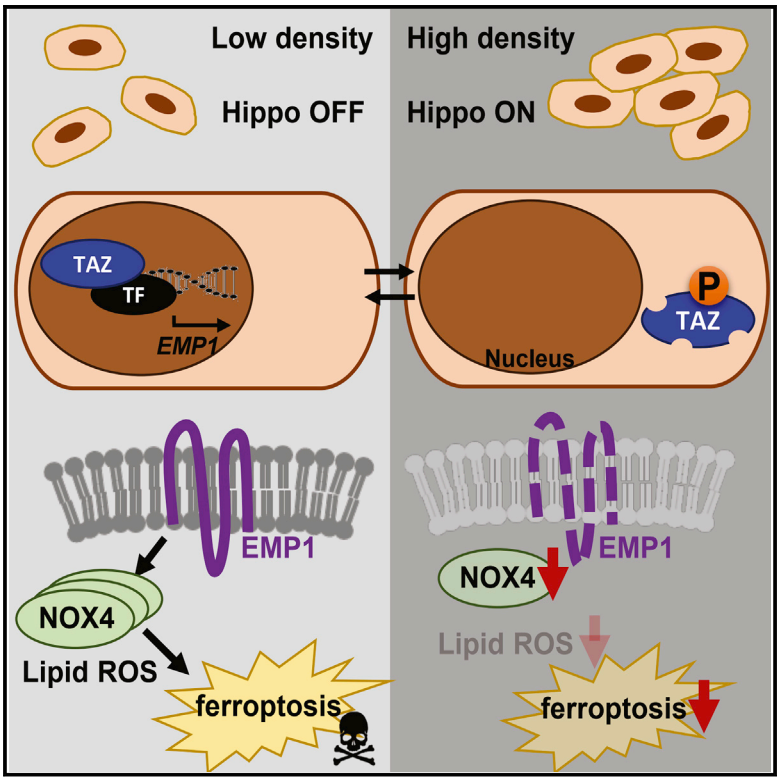

Authors

Wen-Hsuan Yang, Chien-Kuang Cornelia Ding, Tianai Sun, Gabrielle Rupprecht, Chao-Chieh Lin, David Hsu, Jen-Tsan Chi

Correspondence

jentsan.chi@duke.edu

In Brief

Yang et al. show that ferroptosis sensitivity in renal cell carcinoma (RCC) is regulated by cell density through the TAZ-EMP1-NOX4 pathway. These findings reveal TAZ as a genetic determinant of ferroptosis in RCC. In addition, ferroptosis may hold therapeutic potential for RCC and other TAZ-activated tumors.

Highlights

- Ferroptosis susceptibility can be affected by cell density
- TAZ is activated in renal cell carcinoma cell lines and early-passage tumor cells
- The activation status of TAZ regulates the susceptibility of RCC to ferroptosis
- TAZ regulates ferroptosis through affecting EMP1-NOX4 expression

Yang et al., 2019, Cell Reports *28*, 2501–2508
September 3, 2019
https://doi.org/10.1016/j.celrep.2019.07.107

CellPress

Cell Reports
Report

The Hippo Pathway Effector TAZ Regulates Ferroptosis in Renal Cell Carcinoma

Wen-Hsuan Yang,[1,2,3] Chien-Kuang Cornelia Ding,[1,2] Tianai Sun,[1,2] Gabrielle Rupprecht,[2,4] Chao-Chieh Lin,[1,2] David Hsu,[2,4] and Jen-Tsan Chi[1,2,5,*]

[1]Department of Molecular Genetics and Microbiology, Duke University School of Medicine, Durham, NC 27710, USA
[2]Center for Genomic and Computational Biology, Duke University School of Medicine, Durham, NC 27710, USA
[3]Department of Biochemistry, Duke University School of Medicine, Durham, NC 27710, USA
[4]Department of Medicine, Duke University School of Medicine, Durham, NC 27710, USA
[5]Lead Contact
*Correspondence: jentsan.chi@duke.edu
https://doi.org/10.1016/j.celrep.2019.07.107

SUMMARY

Despite recent advances, the poor outcomes in renal cell carcinoma (RCC) suggest novel therapeutics are needed. Ferroptosis is a form of regulated cell death, which may have therapeutic potential toward RCC; however, much remains unknown about the determinants of ferroptosis susceptibility. We found that ferroptosis susceptibility is highly influenced by cell density and confluency. Because cell density regulates the Hippo-YAP/TAZ pathway, we investigated the roles of the Hippo pathway effectors in ferroptosis. TAZ is abundantly expressed in RCC and undergoes density-dependent nuclear or cytosolic translocation. TAZ removal confers ferroptosis resistance, whereas overexpression of TAZS89A sensitizes cells to ferroptosis. Furthermore, TAZ regulates the expression of Epithelial Membrane Protein 1 (EMP1), which, in turn, induces the expression of nicotinamide adenine dinucleotide phosphate (NADPH) Oxidase 4 (NOX4), a renal-enriched reactive oxygen species (ROS)-generating enzyme essential for ferroptosis. These findings reveal that cell density-regulated ferroptosis is mediated by TAZ through the regulation of EMP1-NOX4, suggesting its therapeutic potential for RCC and other TAZ-activated tumors.

INTRODUCTION

Renal cell carcinoma (RCC) annually affects ~338,000 new cases worldwide (Medina-Rico et al., 2018). Despite recent inclusion of anti-angiogenic agents or immune checkpoint inhibition for treating RCC, the median overall survival rate for patients remains unsatisfactory (Hsieh et al., 2017). Thus, identifying new therapeutics is urgent. RCC cells are particularly susceptible to ferroptosis, a form of iron-dependent programmed death that is morphologically, genetically, and biochemically distinct from other cell deaths (Dixon et al., 2012; Yang et al., 2014a), suggesting its therapeutic potential for RCC. Ferroptosis can be induced by erastin (Dolma et al., 2003), which inhibits the glutamate-cystine antiporter system, xCT, resulting in the redox imbalance by decreasing intracellular glutathione (GSH) levels and accumulation of lipid reactive oxygen species (ROS). Lipid ROS can be accumulated by either impaired detoxification of lipid peroxidation via reducing the expression of glutathione peroxidase 4 (GPX4) (Yang et al., 2014a) or by the generation of superoxide and hydrogen peroxide involving upregulation of nicotinamide adenine dinucleotide phosphate (NADPH) oxidases (NOXs) (Dixon et al., 2012). In kidney, NOX4 is highly expressed as an important source of renal ROS (Gorin et al., 2005; Sedeek et al., 2013). In addition, inhibition of NOX4 reduces the cystine deprivation-induced cell death and lipid ROS, suggesting its essential role in ferroptosis (Poursaitidis et al., 2017). However, much remains unknown about the genetic determinants of ferroptosis in RCC.

Here, we demonstrate how cell density regulates the ferroptosis sensitivity of RCC. We found that the Hippo pathway regulator WW Domain Containing Transcription Regulator 1 (TAZ) regulates ferroptosis through Epithelial Membrane Protein 1 (EMP1)-NOX4, implying that ferroptosis can be a therapeutic approach for RCC and other TAZ-activated tumors.

RESULTS

Cell Density Affects the Ferroptosis Sensitivity of RCC Cell Lines

RCCs are susceptible to ferroptosis induced by erastin and cystine deprivation (Tang et al., 2016; Yang et al., 2014a). We found that erastin sensitivity is determined by cell density. When RCC4, a renal cancer cell line, was grown at low cell density (<50% confluency), it was highly sensitive to erastin-induced ferroptosis as the morphological change of cell rounding shown under light microscopy. In contrast, when cells were grown at high cell density (>80% confluency), they became less sensitive to erastin (Figure 1A). Next, we used a cell viability assay to define the erastin 50% effective concentration (EC_{50}) of high or low densities and found high density is associated with >2-fold increases of EC_{50} on both days 1 (Figure 1B) and 3 (Figure S1A). The cell density-regulated ferroptosis sensitivity was further validated by SYTOX Green cell death assay (Figure 1C) and crystal violet staining (Figure S1B).

To exclude the possibility that the differences in cell death under high/low densities were due to the availability of erastin to its target, xCT, we conducted two experiments. First, we seeded

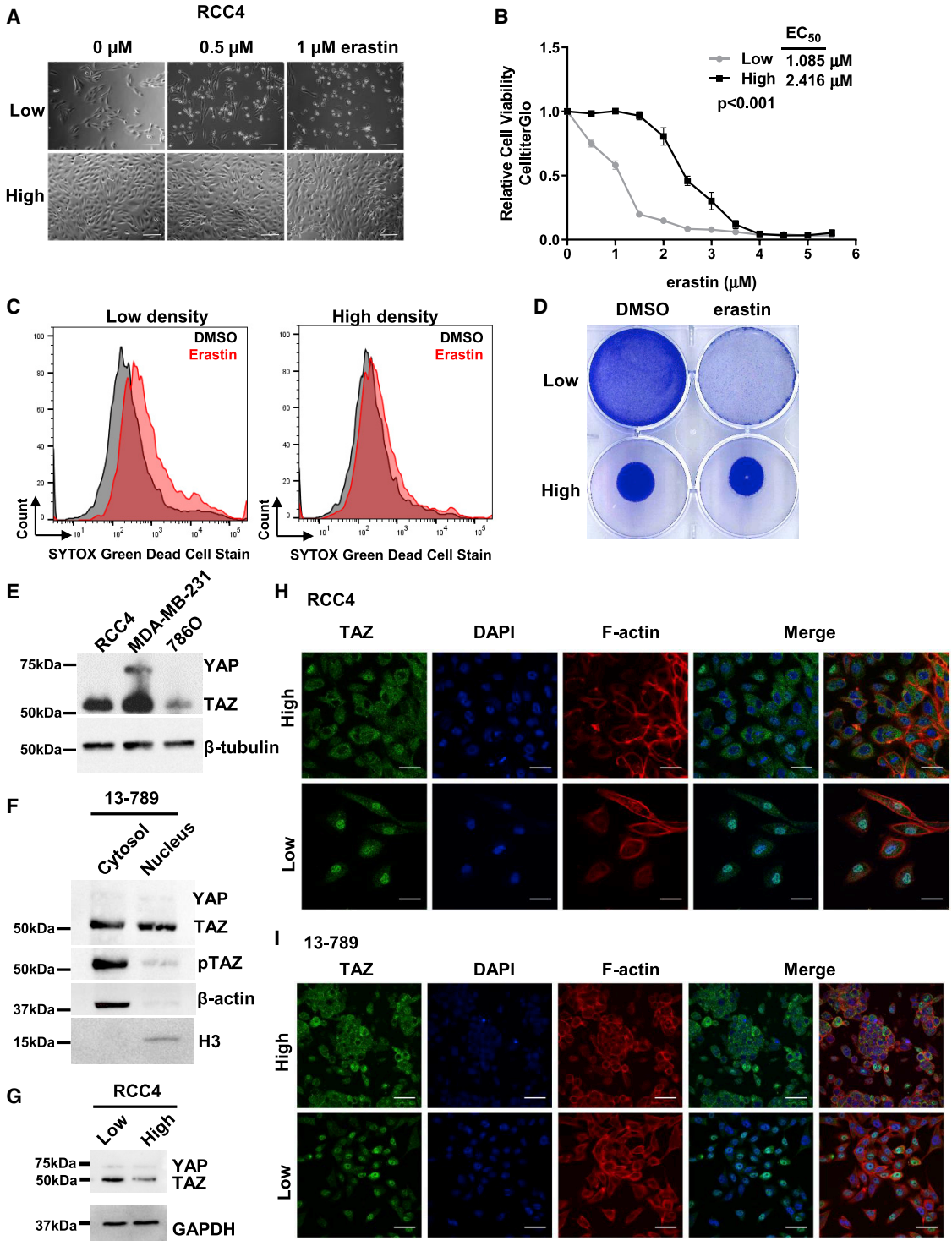

Figure 1. Cell Density Regulates the Ferroptosis Sensitivity of RCC

(A) Bright-field images of RCC4 cells cultured in low/high densities with 0 to 1 μM erastin; n = 3; scale bar, 200 μm.

(B) CelltiterGlo assay and EC_{50} after RCC4 cells of low/high densities treated with erastin for 24 h; n = 3; mean ± SEM; two-way ANOVA.

(C) Cell death assay of RCC4 grown at low/high densities treated with DMSO or 4 μM erastin for 16 h; n = 2.

(D) Crystal violet staining of RCC4 cultured in low/high densities treated with DMSO or 2 μM erastin; n = 3.

(E) Protein expression of YAP and TAZ; n = 3.

(F) YAP/TAZ and phospho-TAZ (Ser89) expressions in cytosol and/or nucleus of RCC PDX 13-789 cells. H3, nuclear marker; β-actin, cytosolic marker.

(legend continued on next page)

the same number of cells in a larger or smaller area to represent low or high cell densities. Crystal violet staining and quantification (Figures 1D and S1C) revealed that the RCC4 cells seeded at high cell density are more resistant to erastin. Second, the upregulation of *CHAC1* gene has been reported as a biomarker for inhibition of xCT by erastin (Dixon et al., 2014). We found comparable *CHAC1* upregulation under high/low densities (Figure S1D). Cell density-dependent erastin sensitivities were also found in human embryonic kidney cells, 293T (Figure S1E), and an early passaged, patient-derived xenograft (PDX) RCC cell line, 13-789 (Figure S1F). To exclude the possibility that cell density alters the mode of cell death induced by erastin, we found that the erastin-induced cell death in low cell density can be rescued by ferrostatin-1, but not by Z-VAD-FMK (Figure S1G). In addition, the cell density also affects the ferroptosis triggered by RSL3, a GPX4 inhibitor (Figure S1H). Together, these data indicate that cell density regulates ferroptosis sensitivity.

The Hippo pathway regulators, YAP and TAZ, are molecular sensors that regulate the density-dependent proliferation of cancer cells (Mori et al., 2014; Zhao et al., 2007). Thus, we investigated the role of YAP and TAZ in ferroptosis. First, we determined the expression of YAP and TAZ proteins in RCC4, 786O, and PDX 13-789 cell lines. With MDA-MB-231 as a control, we found that TAZ protein, but not YAP, was the predominant co-activator in RCC (Figures 1E and 1F). In addition, knockdown of TAZ in RCC4 and 293T cells increased YAP expression, suggesting a compensatory mechanism between TAZ and YAP (Figure S1J).

YAP/TAZ activities are regulated by their phosphorylation and intracellular localization. In high density, YAP and TAZ are phosphorylated, cytosolically retained, and subjected to proteasomal degradation; in low density, YAP and TAZ become dephosphorylated and translocate into the nuclei to associate with TEAD protein to drive gene expression regulating cell proliferation, differentiation, and migration (Hsiao et al., 2016; Zhao et al., 2007). When the expression levels of TAZ in RCC4 were compared between different densities, higher cell density led to a lower level of TAZ protein (Figure 1G). In addition, when RCC4 and PDX 13-789 cells were shifted from high density to low density *in vitro*, TAZ translocated from cytosol to the nuclei (Figures 1H and 1I). To verify that the activated TAZ expression also occurred *in vivo*, we performed cytosolic and nuclear fractionations of RCC PDX tissues. As shown in Figures 1F and S1I, the combination of nuclear TAZ expression with a low level of phosphorylation indicated that TAZ was activated in the PDX 13-789 model. Thus, these results suggest that TAZ is the predominant Hippo effector in RCC, and its subcellular localization is regulated by cell density. Consistent with the ferroptosis sensitivity of RCC, RCC cell lines and renal tumors express the highest level of *WWTR1* mRNA (encoding TAZ) from the analysis of the Cancer Cell Line Encyclopedia (CCLE) and The Cancer Genome Atlas (TCGA) (Figures S1K and S1L). Therefore, we focused on TAZ as the main Hippo effector that regulates ferroptosis in RCC cells.

TAZ Regulates Sensitivity to Erastin-Induced Ferroptosis

To investigate whether TAZ regulates ferroptosis, we found that TAZ knockdown (Figure 2A) reduces erastin-induced death (Figures 2B and 2C). TAZ knockdown in the low-density RCC4 cells also conferred ferroptosis resistance as in high cell density (Figure 2D), suggesting that TAZ activation contributes to the density-dependent ferroptosis sensitivity. Moreover, knockdowns of TAZ in RCC4 by multiple independent small interfering RNAs (siRNAs) all reduce sensitivity to erastin (Figures 2E and S2A). Similar reduced erastin sensitivities by TAZ knockdown were also observed in other RCC cells (786O and 13-789) (Figures 2F, 2G, S2B, and S2C) and breast cancer cells MDA-MB-231 (Figures S2D–S2H), suggesting the general relevance of TAZ for ferroptosis. Conversely, the expression of a constitutively active form of TAZ, TAZS89A (Lei et al., 2008), increased sensitivity to erastin (Figures 2H and 2I). Together, these data indicate that the activation status of TAZ regulates the ferroptosis sensitivities under different cell density.

To characterize the *in vivo* relevance of TAZ-regulated ferroptosis, we determined how the TAZ knockdown (Figure S2I) affects the erastin response of 786O xenografts. Erastin administration reduced the tumor growth in the control 786O xenografts, but not in the TAZ knockdown xenografts (Figures 2J and 2K). The effects of TAZ knockdown on erastin sensitivity were further tested *ex vivo* by 3D Matrigel culture. We found that erastin decreases the sphere size of the control 786O, but not TAZ-knockdown cells (Figures S2J and S2K). These data support the *in vivo* relevance of ferroptosis regulation by TAZ.

EMP1 Is a Direct Target Gene of TAZ That Regulates Ferroptosis Sensitivity

Next, we sought to identify how TAZ regulates erastin sensitivity in RCC4. TAZ is a transcriptional coactivator that affects phenotypes through gene expression. Based on the assumption that TAZ silencing may repress genes essential for ferroptosis, we focused on genes that were both repressed during TAZ knockdown (microarray) and essential for the cystine-deprived death of RCC4 (RNAi screen) (Figures 3A, S3A, and S3B). From these comparisons, we identified 11 candidate genes, including TAZ. After excluding TAZ and two other genes encoding only one subunit of multi-component complexes, we prioritized the eight remaining candidate genes. First, we used qRT-PCR to validate their downregulation upon TAZ removal (Figure S3C). Second, we determined whether each candidate gene was essential for ferroptosis in RCC4 (Figure S3D). Based on these criteria, the epithelial membrane protein 1 (EMP1) emerged as the most promising candidate. *EMP1* mRNA was downregulated upon TAZ knockdown (Figure 3B). In addition, the expression of *EMP1* mRNA was strongly correlated with the expression of

(G) Protein expression of YAP and TAZ of RCC4 at low/high densities; n = 3.
(H and I) Confocal immunofluorescence images of TAZ in RCC4 cells (H) or RCC PDX 13-789 cells (I), when grown at low/high densities. DAPI, nuclei; F actin, cell boundaries. Scale bars, 50 μm.
See also Figure S1.

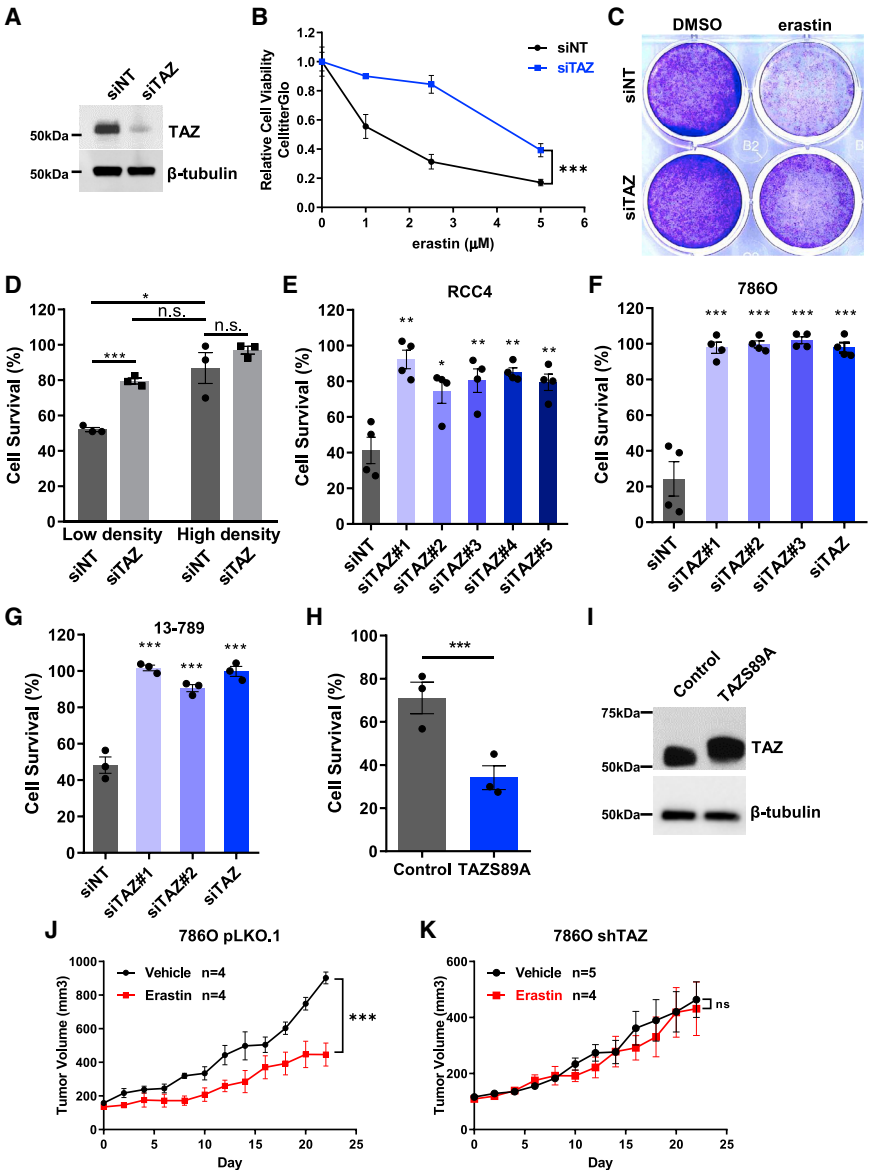

Figure 2. TAZ Regulates Sensitivity to Erastin-Induced Ferroptosis

(A) Control (siNT) or TAZ-targeting (siTAZ) siRNAs knockdown check by western blot in RCC4 cells.

(B) CelltiterGlo assay of siTAZ with erastin; n = 3; mean ± SEM; two-way ANOVA.

(C) Crystal violet staining of RCC4 treated with 1 μM erastin and siNT or siTAZ; n = 2.

(D) CelltiterGlo assay of RCC4 cells transfected with either siNT or siTAZ and seeded in low/high densities. Data are represented as means ± SEM, n = 3 by comparing 1 μM erastin to the DMSO controls of each group; two-way ANOVA.

(E–G) The relative viability of cells transfected with multiple individual siRNAs targeting TAZ (1–5), siTAZ (pooled), or siRNA control (siNT) for 2 days in RCC4 cells (E), 786O cells (F), or RCC PDX 13-789 cells (G). Cell viability was then determined by CelltiterGlo after 24 h treatment of 2.5, 1, and 16 μM of erastin, respectively. Data represented are mean ± SEM and by comparing to the DMSO controls of each group; one-way ANOVA.

(H and I) Overexpression of TAZS89A plasmid sensitizes RCC4 cells to erastin-induced ferroptosis. (H) CelltiterGo assay; data represented are mean ± SEM, n = 3 by comparing 4 μM erastin to the DMSO controls; Student's t test (I) protein expression of TAZ.

(J and K) 786O cells transduced with either control (pLKO.1) (J) or TAZ-targeting short hairpin RNA (shRNA; shTAZ) (K) were injected subcutaneously, and the tumor volume was determined at the indicated time; two-way ANOVA.

*p < 0.05; **p < 0.01; ***p < 0.001; ns, not significant. See also Figure S2.

CTGF and *CYR61* mRNAs, two well-known YAP/TAZ target genes in TCGA (Figures S3E and S3F) and CCLE (Figures S3G and S3H). EMP1 knockdown by multiple siRNAs also conferred ferroptosis resistance in RCC4 (Figures 3C and S3I), 786O (Figures 3D and S3J), and MDA-MB-231 cells (Figures S3K and S3L). Thus, the downregulation of EMP1 may contribute to the ferroptosis resistance conferred by the TAZ knockdown. Conversely, overexpression of EMP1 sensitizes RCC4 to erastin (Figures 3E and S3M). Furthermore, EMP1 overexpression reduces the ferroptosis protection conferred by TAZ knockdown (Figure 3F), indicating that EMP1 genetically works downstream of TAZ to regulate ferroptosis.

Previous chromatin immunoprecipitation sequencing (ChIP-seq) studies have suggested that the regulatory regions of EMP1 were physically associated with YAP/TAZ/TEAD complexes (Stein et al., 2015; Walko et al., 2017; Zanconato et al., 2015). To validate that EMP1 is a direct target gene of TAZ, we performed ChIP-qPCR using an antibody specific for endogenous TAZ protein. As shown in Figure 3G, EMP1 was enriched in the TAZ pull-down as the positive control connective tissue growth factor (CTGF), indicating that EMP1 promoter is directly associated with TAZ. Together, these data support EMP1 as a direct target gene of TAZ that regulates ferroptosis sensitivity.

EMP1 Regulates Ferroptosis through NOX4

To investigate the mechanistic link between EMP1 and ferroptosis, we sought to determine whether EMP1 would affect the levels of GPX4 or NOX4, two key regulators of lipid peroxidation for ferroptosis (Dixon et al., 2012; Poursaitidis et al., 2017; Yang et al., 2014a). We found that EMP1 knockdown decreased the mRNA expression of NOX4, but not GPX4 (Figures 4A, S4A, and S4B). Conversely, EMP1 overexpression increases the mRNA level of NOX4, but not GPX4 (Figures 4B, S4C, and S4D). Overexpression of EMP1 also increases NOX4 protein level (Figure 4C), but not GPX4 protein level (Figure S4E). Thus, we reasoned that EMP1 may regulate ferroptosis by affecting the levels and activities of NOX4. Consistent with its ability to

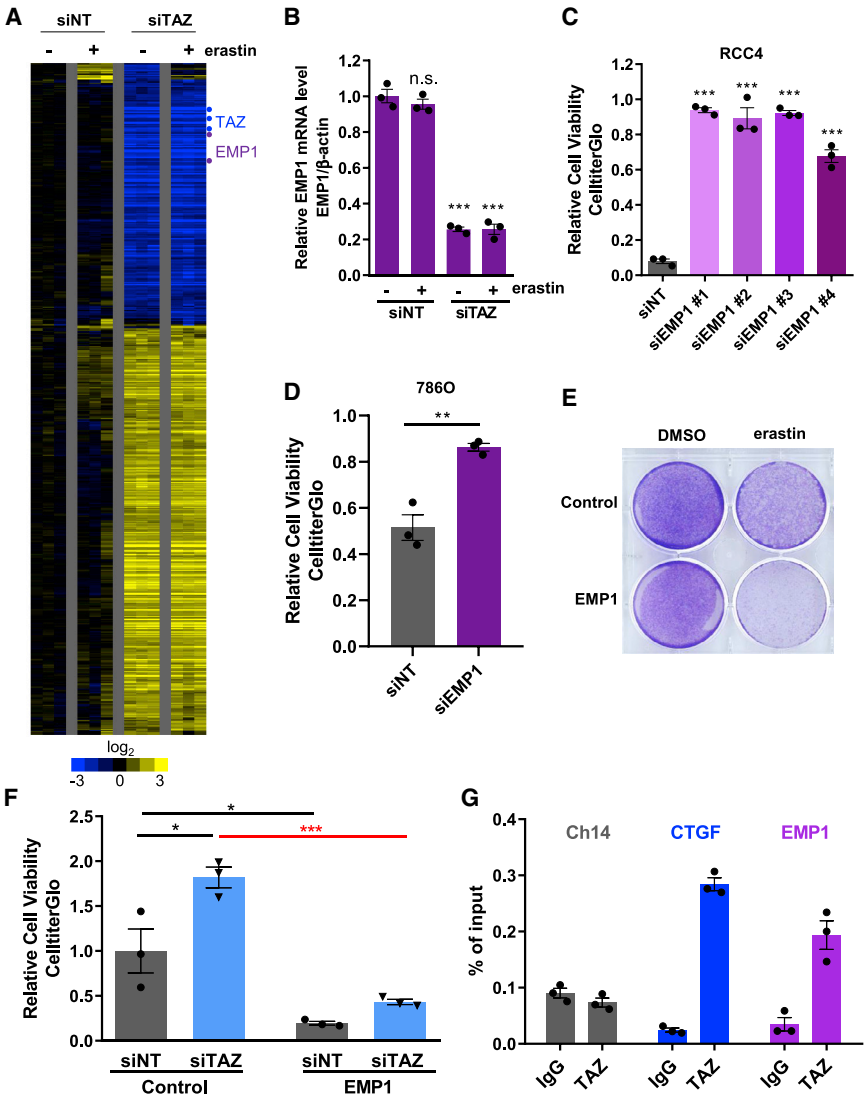

Figure 3. EMP1 Is a Direct Target Gene of TAZ That Regulates Ferroptosis Sensitivity

(A) Microarray of RCC4 cells treated with 1 μM erastin for 7 h after either siNT or siTAZ.

(B) qRT-PCR validates EMP1 as being down-regulated when TAZ is knock downed by siRNAs. Data represented are mean ± SEM, n = 3 after normalized to the DMSO controls; one-way ANOVA.

(C) siRNAs targeting EMP1 reduce erastin-induced ferroptosis. CelltiterGlo assays are represented as mean ± SEM, n = 3 by comparing 2 μM erastin to the DMSO controls; one-way ANOVA.

(D) EMP1 knockdown reduces erastin-induced ferroptosis in 786O cells. CelltiterGlo data are represented as mean ± SEM, n = 3 by comparing 1 μM erastin to the DMSO controls; Student's t test.

(E) Overexpression EMP1 sensitizes RCC4 cells to ferroptosis. Crystal violet staining of RCC4 cells that stably overexpress control vector (pLX304) or pLX304-EMP1-V5 (EMP1) after treatment with 3 μM erastin for 1 day.

(F) Genetic interaction between TAZ and EMP1. After stably overexpressing with EMP1, RCC4 cells were treated with siTAZ. CelltiterGlo data represented are mean ± SEM, n = 3 after normalized with 2 μM erastin to the DMSO controls; two-way ANOVA.

(G) EMP1 is the direct target of TAZ. From RCC4 lysates, ChIP-qPCR with TAZ antibody validates the finding that TAZ binds to the EMP1 promoter. ChIP-qPCR of the CTGF promoter serves as a positive control, whereas Ch14 serves as a negative control. Data from three technical replicates, mean ± SEM, from one representative out of four experiments, are shown.

*p < 0.05; **p < 0.01; ***p < 0.001; ns, not significant. See also Figure S3.

induce EMP1, TAZS89A also increased the level of NOX4 protein (Figure S4F), but not GPX4 (Figure S4E). To rule out that elevated NOX4 may affect ferroptosis through GSH, we measured the GSH levels when the control and TAZ-knockdown cells were exposed to erastin. We found that erastin treatments significantly reduced the GSH levels (Figure S4G), as previously reported (Yang et al., 2014a). However, the TAZ knockdown did not affect the GSH levels before or after erastin treatments (Figure S4G). We further found that the NOX1/NOX4 inhibitor, GKT136901 (Laleu et al., 2010), protected RCC4 from ferroptosis (Figure 4D). Because NOX1 was not detectable in RCC cell lines (Gregg et al., 2014), GKT136901 probably mediated the ferroptosis protection through NOX4. Consistently, knockdowns of NOX4 by siRNAs also conferred ferroptosis resistance (Figures 4E and S4H). Conversely, overexpression of NOX4 increased the sensitivity of RCC4 to erastin treatment (Figures S4I–S4K). To investigate the genetic interaction between EMP1 and NOX4, we treated the NOX4 inhibitor, GKT136901, in EMP1-overexpressing RCC4. We found that the EMP1 overexpression increased erastin sensitivity, but that increased sensitivity was abolished by GKT136901 (Figure 4F).

As p38 mitogen-activated protein kinase (MAPK) has been reported to regulate NOX4 reciprocally (Dougherty et al., 2017; Huang et al., 2018; Park et al., 2010; Peng et al., 2013), we examined the role of p38 activity in the NOX4 induction by EMP1. We found that EMP1 expression increased the phosphorylation and activation of p38 (Figure 4G). Furthermore, EMP1 silencing reduced the p38 phosphorylation (Figure 4H). In addition, a p38 inhibitor, SB203580, abrogated the increase of NOX4 associated with EMP1 expression (Figure 4I).

Finally, we measured the lipid ROS, which is crucial for ferroptosis (Dixon et al., 2012), by C11-BODIPY staining. We found that the erastin-induced accumulation of lipid ROS is abolished by knockdown of TAZ, knockdown of EMP1, or NOX4 inhibitor, GKT136901 (Figures 4J and S4L). Taken together, we propose a molecular model (Figure 4K) by which TAZ regulates cell

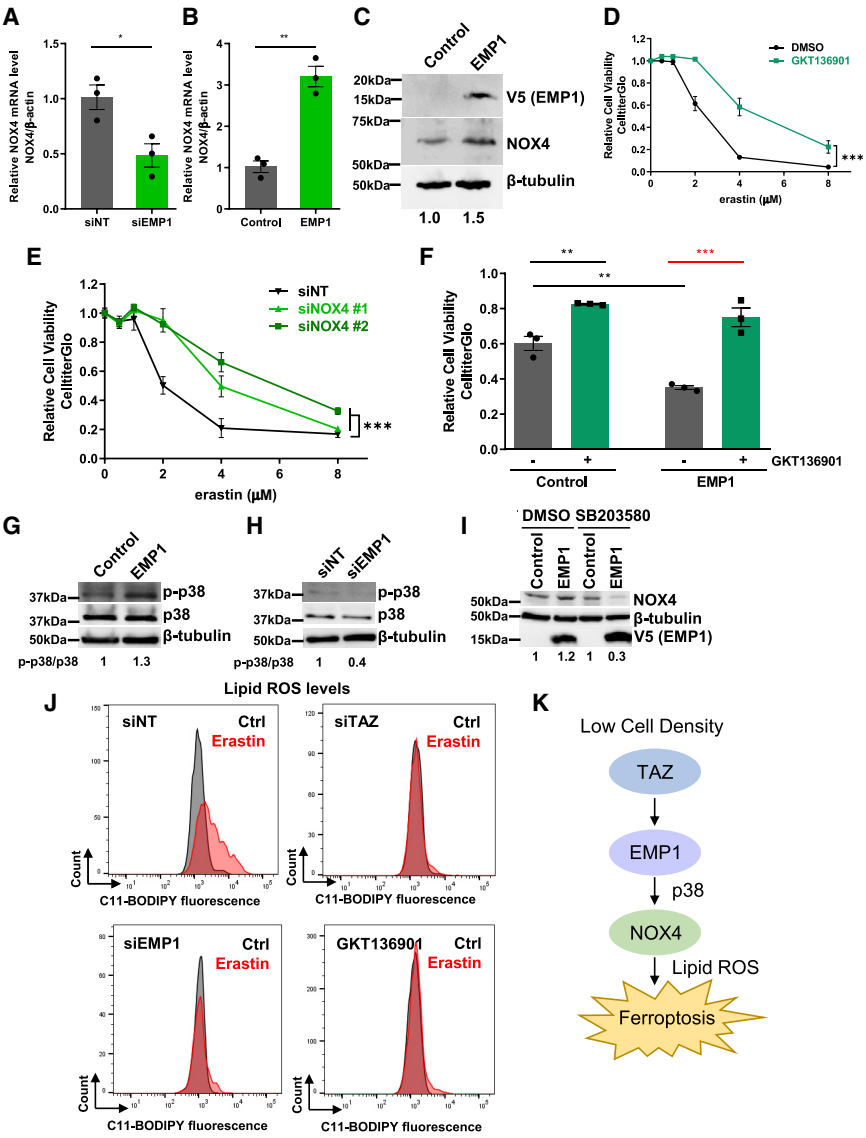

Figure 4. EMP1 Regulates Ferroptosis through NOX4

(A) siRNA-mediated knockdown of EMP1 gene reduces the mRNA level of NOX4; n = 3; mean ± SEM; Student's t test.

(B) Overexpression of EMP1 increases NOX4 mRNA level; n = 3; mean ± SEM; Student's t test.

(C) Overexpression of V5-EMP1 elevates NOX4 protein. V5 antibody indicated EMP1-V5 overexpression. The western blots of NOX4 were quantified, normalized to the β-tubulin, and relative to the control vector, as shown in the numbers below. Representative data from one of at least three independent studies.

(D and E) Inhibition of NOX4 reduces erastin-induced ferroptosis. Cell viability was determined by CelltiterGlo after 1 day at the indicated concentrations of erastin with (D) NOX4 inhibitor, 10 μM GKT136901; mean ± SEM; n = 3; two-way ANOVA; and (E) silencing NOX4 by two individual siRNAs; mean ± SEM; n = 3; Data are represented by being compared with the DMSO controls; two-way ANOVA.

(F) Genetic interaction between EMP1 and NOX4. Cell viabilities were determined by CelltiterGlo after RCC4 cells were treated with an EMP1 expression construct for 1 day after 20 μM GKT136901 and 8 μM erastin for 1 day. Data represented are mean ± SEM, n = 3 after normalized to the DMSO controls; two-way ANOVA.

(G and H) Western blot analysis of phospho-p38 (Thr180/Tyr182), total p38, and control β-tubulin upon overexpression of EMP1 (G) or siRNA-mediated silencing of EMP1 (H). Densitometry analyses phospho-p38 normalized to p38 were shown below the corresponding blots.

(I) Western blot analysis of NOX4 upon overexpression of EMP1 with treatment of p38 inhibitor, SB203580. Quantification of the ratio of NOX4 to β-tubulin was normalized to the DMSO control.

(J) Inhibition of TAZ, EMP1, or NOX4 abolishes the elevated lipid ROS induced by erastin treatment. Lipid ROS in RCC4 cells was assessed by flow cytometry with C11-BODIPY after being transfected with siTAZ or siEMP1 or treated with NOX4 inhibitor. Representative data from one of five independent experiments are shown.

(K) A schematic model illustrating the erastin-induced ferroptosis regulated by the TAZ-EMP1-NOX4 axis.

*p < 0.05; **p < 0.01; ***p < 0.001; ns, not significant. See also Figure S4.

density-dependent ferroptosis by affecting the levels of EMP1, which, in turn, regulates NOX4, lipid peroxidation, and ferroptotic death of RCC.

DISCUSSION

Previous studies of ferroptosis have identified certain genetic determinants (Chen et al., 2019; Ding et al., 2018; Dixon et al., 2012), but the role of non-genetic factors are unknown. Here, we identify that a non-genetic factor, cell density, regulates ferroptosis sensitivity. A similar observation is also reported on *BioRxiv* (Panzilius et al., 2018). Importantly, we have elucidated the molecular mechanism by which cell density regulates ferroptosis in RCC; TAZ affects the levels of EMP1, NOX4, and resulting lipid peroxidation and ferroptosis. Therefore, TAZ activation may promote ferroptosis and predict of ferroptosis sensitivity.

Although our current study focuses on the regulation of ferroptosis by TAZ, the relevant roles of other components of the Hippo pathway remain unknown. For example, YAP may also regulate ferroptosis in cells with a high level of YAP protein. Furthermore, the Hippo pathway integrates a wide variety of non-genetic factors, such as mechanical properties and metabolic status (Zanconato et al., 2016). Therefore, our findings may suggest that these Hippo-sensitive, non-genetic factors may also regulate ferroptosis sensitivities. For example, epithelial-mesenchymal transition and fibrosis are prominent features of RCC, which

may lead to the "stiff" environment known to activate the YAP/TAZ and promote ferroptosis. In addition, YAP/TAZ is also regulated by metabolic pathways, which may help to explain the essential role of glutamine metabolism in ferroptosis (Gao et al., 2015).

Although inducing ferroptosis may have anti-tumor potential, it is important to identify genetic influences on the response to those ferroptosis-inducing agents. Our results suggest that TAZ-activated tumors may be particularly responsive. Previous studies have revealed that chemo-resistant persister cells are highly sensitive to ferroptosis, based on a high level of GPX4 (Hangauer et al., 2017; Viswanathan et al., 2017). The drug resistance and persister cells are also known to be associated with YAP/TAZ activation (Lin et al., 2015; Zanconato et al., 2016) and EMP1 expression (Jain et al., 2005). Our results suggest that TAZ-EMP1-NOX4 and ZEB1-GPX4 may represent two distinct pathways linking the chemo-resistance with ferroptosis, which may operate in different resistant settings.

Besides cancer, ferroptosis also has emerging roles in other pathophysiological processes and diseases, such as neurotoxicity (Skouta et al., 2014), acute renal failure (Friedmann Angeli et al., 2014), cardiac injury (Gao et al., 2015), and ischemia-reperfusion injury (Linkermann et al., 2014). Therefore, modulating ferroptosis may have therapeutic potentials. In addition, the ability of NOX4 inhibitors to abolish ferroptosis suggests the potential for developing combinational therapies. Currently, several oral NOX4 inhibitors are under preclinical studies (Borbély et al., 2010) and may be tested for their efficacy in mitigating these ferroptosis-associated diseases.

STAR★METHODS

Detailed methods are provided in the online version of this paper and include the following:

- KEY RESOURCES TABLE
- LEAD CONTACT AND MATERIALS AVAILABILITY
- MATERIALS AVAILABILITY STATEMENT
- EXPERIMENTAL MODEL AND SUBJECT DETAILS
  - Cell Culture Studies
  - Animal Models
  - Patient-Derived Xenograft
- METHOD DETAILS
  - Determine of cell viability, cell death, and glutathione level
  - Western blot analysis
  - RNA isolation and quantitative real-time PCR
  - Microarray
  - Immunofluorescence staining
  - ChIP analysis
  - Lipid ROS assay using flow cytometry
- QUANTIFICATION AND STATISTICAL ANALYSIS
- DATA AND CODE AVAILABILITY

SUPPLEMENTAL INFORMATION

Supplemental Information can be found online at https://doi.org/10.1016/j.celrep.2019.07.107.

ACKNOWLEDGMENTS

We thank Bettie Sue Masters and Po-Han Chen for their critical feedback as well as Wayne Glove, Hsin-I Huang, Mike Cook, and Benjamin Carlson for technical assistance. This work was supported by DOD (W81XWH-17-1-0143, W81XWH-15-1-0486, and KC180120) and the NIH (R01GM124062 and 1R01NS111588) to J.-T.C.

AUTHOR CONTRIBUTIONS

W.-H.Y. and J.-T.C. conceived the project, designed the experiments, and wrote the manuscript. All other authors edited and commented on the manuscript. J.-T.C. secured funding and supervised the research. D.H. designed the mice study and provided the PDX cell line. W.-H.Y. and G.R. performed the mice study. W.-H.Y. performed cell experiments and analyzed the data with assistance from C.-K.C.D., C.-C.L., and T.S.

DECLARATION OF INTERESTS

The authors declare no competing interests.

Received: December 21, 2018
Revised: June 28, 2019
Accepted: July 22, 2019
Published: September 3, 2019

REFERENCES

Borbély, G., Szabadkai, I., Horváth, Z., Markó, P., Varga, Z., Breza, N., Baska, F., Vántus, T., Huszár, M., Geiszt, M., et al. (2010). Small-molecule inhibitors of NADPH oxidase 4. J. Med. Chem. *53*, 6758–6762.

Chen, P.-H., Wu, J., Ding, C.C., Lin, C.-C., Pan, S., Bossa, N., Xu, Y., Yang, W.-H., Mathey-Prevot, B., and Chi, J.-T. (2019). Kinome screen of ferroptosis reveals a novel role of ATM in regulating iron metabolism. Cell Death Differ. Published online July 18, 2019. https://doi.org/10.1038/s41418-019-0393-7.

Ding, C.-K.C., Rose, J., Wu, J., Sun, T., Chen, K.-Y., Chen, P.-H., Xu, E., Tian, S., Akinwuntan, J., Guan, Z., et al. (2018). Mammalian stringent-like response mediated by the cytosolic NADPH phosphatase MESH1. bioRxiv. https://doi.org/10.1101/325266.

Dixon, S.J., Lemberg, K.M., Lamprecht, M.R., Skouta, R., Zaitsev, E.M., Gleason, C.E., Patel, D.N., Bauer, A.J., Cantley, A.M., Yang, W.S., et al. (2012). Ferroptosis: an iron-dependent form of nonapoptotic cell death. Cell *149*, 1060–1072.

Dixon, S.J., Patel, D.N., Welsch, M., Skouta, R., Lee, E.D., Hayano, M., Thomas, A.G., Gleason, C.E., Tatonetti, N.P., Slusher, B.S., and Stockwell, B.R. (2014). Pharmacological inhibition of cystine-glutamate exchange induces endoplasmic reticulum stress and ferroptosis. eLife *3*, e02523.

Dolma, S., Lessnick, S.L., Hahn, W.C., and Stockwell, B.R. (2003). Identification of genotype-selective antitumor agents using synthetic lethal chemical screening in engineered human tumor cells. Cancer Cell *3*, 285–296.

Dougherty, J.A., Kilbane Myers, J., Khan, M., Angelos, M.G., and Chen, C.-A. (2017). Dual-specificity phosphatase 4 overexpression in cells prevents hypoxia/reoxygenation-induced apoptosis via the upregulation of eNOS. Front. Cardiovasc. Med. *4*, 22.

Friedmann Angeli, J.P., Schneider, M., Proneth, B., Tyurina, Y.Y., Tyurin, V.A., Hammond, V.J., Herbach, N., Aichler, M., Walch, A., Eggenhofer, E., et al. (2014). Inactivation of the ferroptosis regulator Gpx4 triggers acute renal failure in mice. Nat. Cell Biol. *16*, 1180–1191.

Gao, M., Monian, P., Quadri, N., Ramasamy, R., and Jiang, X. (2015). Glutaminolysis and transferrin regulate ferroptosis. Mol. Cell *59*, 298–308.

Gorin, Y., Block, K., Hernandez, J., Bhandari, B., Wagner, B., Barnes, J.L., and Abboud, H.E. (2005). Nox4 NAD(P)H oxidase mediates hypertrophy and fibronectin expression in the diabetic kidney. J. Biol. Chem. *280*, 39616–39626.

Gregg, J.L., Turner, R.M., 2nd, Chang, G., Joshi, D., Zhan, Y., Chen, L., and Maranchie, J.K. (2014). NADPH oxidase NOX4 supports renal tumorigenesis

by promoting the expression and nuclear accumulation of HIF2α. Cancer Res. *74*, 3501–3511.

Hangauer, M.J., Viswanathan, V.S., Ryan, M.J., Bole, D., Eaton, J.K., Matov, A., Galeas, J., Dhruv, H.D., Berens, M.E., Schreiber, S.L., et al. (2017). Drug-tolerant persister cancer cells are vulnerable to GPX4 inhibition. Nature *551*, 247–250.

Hsiao, C., Lampe, M., Nillasithanukroh, S., Han, W., Lian, X., and Palecek, S.P. (2016). Human pluripotent stem cell culture density modulates YAP signaling. Biotechnol. J. *11*, 662–675.

Hsieh, J.J., Purdue, M.P., Signoretti, S., Swanton, C., Albiges, L., Schmidinger, M., Heng, D.Y., Larkin, J., and Ficarra, V. (2017). Renal cell carcinoma. Nat. Rev. Dis. Primers *3*, 17009.

Huang, Y., Cai, G.Q., Peng, J.-P., and Shen, C. (2018). Glucocorticoids induce apoptosis and matrix metalloproteinase-13 expression in chondrocytes through the NOX4/ROS/p38 MAPK pathway. J. Steroid Biochem. Mol. Biol. *181*, 52–62.

Jain, A., Tindell, C.A., Laux, I., Hunter, J.B., Curran, J., Galkin, A., Afar, D.E., Aronson, N., Shak, S., Natale, R.B., and Agus, D.B. (2005). Epithelial membrane protein-1 is a biomarker of gefitinib resistance. Proc. Natl. Acad. Sci. USA *102*, 11858–11863.

Johnson, D.S., Mortazavi, A., Myers, R.M., and Wold, B. (2007). Genome-wide mapping of in vivo protein-DNA interactions. Science *316*, 1497–1502.

Keenan, M.M., Liu, B., Tang, X., Wu, J., Cyr, D., Stevens, R.D., Ilkayeva, O., Huang, Z., Tollini, L.A., Murphy, S.K., et al. (2015). ACLY and ACC1 regulate hypoxia-induced apoptosis by modulating ETV4 via α-ketoglutarate. PLoS Genet. *11*, e1005599.

Kim, M.K., Osada, T., Barry, W.T., Yang, X.Y., Freedman, J.A., Tsamis, K.A., Datto, M., Clary, B.M., Clay, T., Morse, M.A., et al. (2012). Characterization of an oxaliplatin sensitivity predictor in a preclinical murine model of colorectal cancer. Mol. Cancer Ther. *11*, 1500–1509.

Laleu, B., Gaggini, F., Orchard, M., Fioraso-Cartier, L., Cagnon, L., Houngninou-Molango, S., Gradia, A., Duboux, G., Merlot, C., Heitz, F., et al. (2010). First in class, potent, and orally bioavailable NADPH oxidase isoform 4 (Nox4) inhibitors for the treatment of idiopathic pulmonary fibrosis. J. Med. Chem. *53*, 7715–7730.

Lei, Q.Y., Zhang, H., Zhao, B., Zha, Z.Y., Bai, F., Pei, X.H., Zhao, S., Xiong, Y., and Guan, K.L. (2008). TAZ promotes cell proliferation and epithelial-mesenchymal transition and is inhibited by the hippo pathway. Mol. Cell. Biol. *28*, 2426–2436.

Lin, L., Sabnis, A.J., Chan, E., Olivas, V., Cade, L., Pazarentzos, E., Asthana, S., Neel, D., Yan, J.J., Lu, X., et al. (2015). The Hippo effector YAP promotes resistance to RAF- and MEK-targeted cancer therapies. Nat. Genet. *47*, 250–256.

Linkermann, A., Skouta, R., Himmerkus, N., Mulay, S.R., Dewitz, C., De Zen, F., Prokai, A., Zuchtriegel, G., Krombach, F., Welz, P.S., et al. (2014). Synchronized renal tubular cell death involves ferroptosis. Proc. Natl. Acad. Sci. USA *111*, 16836–16841.

Medina-Rico, M., Ramos, H.L., Lobo, M., Romo, J., and Prada, J.G. (2018). Epidemiology of renal cancer in developing countries: review of the literature. Can. Urol. Assoc. J. *12*, E154–E162.

Mori, M., Triboulet, R., Mohseni, M., Schlegelmilch, K., Shrestha, K., Camargo, F.D., and Gregory, R.I. (2014). Hippo signaling regulates microprocessor and links cell-density-dependent miRNA biogenesis to cancer. Cell *156*, 893–906.

Panzilius, E., Holstein, F., Bannier-Hélaouët, M., von Toerne, C., Koenig, A.-C., Hauck, S.M., Ganz, H.M., Angeli, J.P.F., Conrad, M., and Scheel, C.H. (2018). A cell-density dependent metabolic switch sensitizes breast cancer cells to ferroptosis. bioRxiv. https://doi.org/10.1101/417949.

Park, S., Ahn, J.-Y., Lim, M.-J., Kim, M.-H., Yun, Y.-S., Jeong, G., and Song, J.-Y. (2010). Sustained expression of NADPH oxidase 4 by p38 MAPK-Akt signaling potentiates radiation-induced differentiation of lung fibroblasts. J. Mol. Med. (Berl.) *88*, 807–816.

Peng, H., Li, W., Seth, D.M., Nair, A.R., Francis, J., and Feng, Y. (2013). (Pro) renin receptor mediates both angiotensin II-dependent and -independent oxidative stress in neuronal cells. PLoS ONE *8*, e58339.

Poursaitidis, I., Wang, X., Crighton, T., Labuschagne, C., Mason, D., Cramer, S.L., Triplett, K., Roy, R., Pardo, O.E., Seckl, M.J., et al. (2017). Oncogene-selective sensitivity to synchronous cell death following modulation of the amino acid nutrient cystine. Cell Rep. *18*, 2547–2556.

Saldanha, A.J. (2004). Java Treeview—extensible visualization of microarray data. Bioinformatics *20*, 3246–3248.

Sedeek, M., Nasrallah, R., Touyz, R.M., and Hébert, R.L. (2013). NADPH oxidases, reactive oxygen species, and the kidney: friend and foe. J. Am. Soc. Nephrol. *24*, 1512–1518.

Serrander, L., Cartier, L., Bedard, K., Banfi, B., Lardy, B., Plastre, O., Sienkiewicz, A., Fórró, L., Schlegel, W., and Krause, K.H. (2007). NOX4 activity is determined by mRNA levels and reveals a unique pattern of ROS generation. Biochem. J. *406*, 105–114.

Skouta, R., Dixon, S.J., Wang, J., Dunn, D.E., Orman, M., Shimada, K., Rosenberg, P.A., Lo, D.C., Weinberg, J.M., Linkermann, A., and Stockwell, B.R. (2014). Ferrostatins inhibit oxidative lipid damage and cell death in diverse disease models. J. Am. Chem. Soc. *136*, 4551–4556.

Stein, C., Bardet, A.F., Roma, G., Bergling, S., Clay, I., Ruchti, A., Agarinis, C., Schmelzle, T., Bouwmeester, T., Schübeler, D., and Bauer, A. (2015). YAP1 exerts its transcriptional control via tead-mediated activation of enhancers. PLoS Genet. *11*, e1005465.

Tang, X., Wu, J., Ding, C.K., Lu, M., Keenan, M.M., Lin, C.C., Lin, C.A., Wang, C.C., George, D., Hsu, D.S., and Chi, J.T. (2016). Cystine deprivation triggers programmed necrosis in VHL-deficient renal cell carcinomas. Cancer Res. *76*, 1892–1903.

Tang, X., Ding, C.K., Wu, J., Sjol, J., Wardell, S., Spasojevic, I., George, D., McDonnell, D.P., Hsu, D.S., Chang, J.T., and Chi, J.T. (2017). Cystine addiction of triple-negative breast cancer associated with EMT augmented death signaling. Oncogene *36*, 4379.

Uronis, J.M., Osada, T., McCall, S., Yang, X.Y., Mantyh, C., Morse, M.A., Lyerly, H.K., Clary, B.M., and Hsu, D.S. (2012). Histological and molecular evaluation of patient-derived colorectal cancer explants. PLoS ONE *7*, e38422.

Viswanathan, V.S., Ryan, M.J., Dhruv, H.D., Gill, S., Eichhoff, O.M., Seashore-Ludlow, B., Kaffenberger, S.D., Eaton, J.K., Shimada, K., Aguirre, A.J., et al. (2017). Dependency of a therapy-resistant state of cancer cells on a lipid peroxidase pathway. Nature *547*, 453–457.

Walko, G., Woodhouse, S., Pisco, A.O., Rognoni, E., Liakath-Ali, K., Lichtenberger, B.M., Mishra, A., Telerman, S.B., Viswanathan, P., Logtenberg, M., et al. (2017). A genome-wide screen identifies YAP/WBP2 interplay conferring growth advantage on human epidermal stem cells. Nat. Commun. *8*, 14744.

Yang, X., Boehm, J.S., Yang, X., Salehi-Ashtiani, K., Hao, T., Shen, Y., Lubonja, R., Thomas, S.R., Alkan, O., Bhimdi, T., et al. (2011). A public genome-scale lentiviral expression library of human ORFs. Nat. Methods *8*, 659–661.

Yang, W.S., SriRamaratnam, R., Welsch, M.E., Shimada, K., Skouta, R., Viswanathan, V.S., Cheah, J.H., Clemons, P.A., Shamji, A.F., Clish, C.B., et al. (2014a). Regulation of ferroptotic cancer cell death by GPX4. Cell *156*, 317–331.

Yang, Z., Nakagawa, K., Sarkar, A., Maruyama, J., Iwasa, H., Bao, Y., Ishigami-Yuasa, M., Ito, S., Kagechika, H., Hata, S., et al. (2014b). Screening with a novel cell-based assay for TAZ activators identifies a compound that enhances myogenesis in C2C12 cells and facilitates muscle repair in a muscle injury model. Mol. Cell. Biol. *34*, 1607–1621.

Zanconato, F., Forcato, M., Battilana, G., Azzolin, L., Quaranta, E., Bodega, B., Rosato, A., Bicciato, S., Cordenonsi, M., and Piccolo, S. (2015). Genome-wide association between YAP/TAZ/TEAD and AP-1 at enhancers drives oncogenic growth. Nat. Cell Biol. *17*, 1218–1227.

Zanconato, F., Cordenonsi, M., and Piccolo, S. (2016). YAP/TAZ at the Roots of Cancer. Cancer Cell *29*, 783–803.

Zhao, B., Wei, X., Li, W., Udan, R.S., Yang, Q., Kim, J., Xie, J., Ikenoue, T., Yu, J., Li, L., et al. (2007). Inactivation of YAP oncoprotein by the Hippo pathway is involved in cell contact inhibition and tissue growth control. Genes Dev. *21*, 2747–2761.

STAR★METHODS

KEY RESOURCES TABLE

REAGENT or RESOURCE	SOURCE	IDENTIFIER
Antibodies		
YAP/TAZ antibody	Cell Signaling Technology	Cat# 8418, RRID:AB_10950494
Phospho-YAP (Ser127) antibody	Cell Signaling Technology	Cat# 4911, RRID:AB_2218913
TAZ antibody	Cell Signaling Technology	Cat#70148, RRID:AB_2799776
β-tubulin antibody	Cell Signaling Technology	Cat# 86298, RRID:AB_2715541
β-actin antibody	Santa Cruz Biotechnology	Cat# sc-130301, RRID:AB_2223360
V5 tag antibody	Thermo Fisher Scientific	Cat# MA5-15253, RRID:AB_10977225
NOX4 antibody	Abcam	Cat# ab133303, RRID:AB_11155321
GPX4 antibody	Abcam	Cat# ab125066, RRID:AB_10973901
Anti-rabbit IgG, HRP-linked antibody	Cell Signaling Technology	Cat# 7074, RRID:AB_2099233
Anti-mouse IgG, HRP-linked antibody	Cell Signaling Technology	Cat# 7076, RRID:AB_330924
Biological Samples		
Patient-derived xenografts (PDX)	Duke University Medical Center	IRB protocol (Pro000022289)
Chemicals, Peptides, and Recombinant Proteins		
Erastin	Duke University Small Molecular Synthesis Facility	Batch DG11_65
Ferrostatin-1	Sigma	SML0583
Z-VAD-FMK	MiliporeSigma	Cat# 627610
Growth factor reduced Matrigel	Corning	Cat#356231
TransIT®-LT1 Transfection Reagent	Mirus Bio	MIR2305
Lipofectamine RNAiMAX Transfection Reagent	Thermo Fisher Scientific	Cat# 13778150
Critical Commercial Assays		
CellTiterGlo™ Luminescent Cell Viability Assay Kit	Promega	Cat# G7571
CytoTox-Fluor Cytotoxicity Assay	Promega	Cat# G9260
GSH/GSSG-Glo Assay	Promega	Cat# V6611
RNAeasy Mini Kit	QIAGEN	Cat# 74104
RNase-Free DNase Set	QIAGEN	Cat# 79254
SuperScript II Reverse Transcriptase	Thermo Fisher Scientific	Cat# 18064014
Power SYBR Green Master Mix	Thermo Fisher Scientific	Cat# 4368577
SYTOX Green Dead Cell Stain	Thermo Fisher Scientific	Cat# S34860
Deposited Data		
siTAZ microarray	This paper	GSE: 121689
Experimental Models: Cell Lines		
RCC4	Denise Chan	Authenticated by DNA Diagnostics Center at Nov 2015
786O	Denise Chan	Authenticated by DNA Diagnostics Center at Nov 2015
HEK293T	Duke Cell Culture Facility	CRL-11268 RRID: CVCL_1926
MDA-MB-231	Duke Cell Culture Facility	HTB-26 RRID:CVCL_0062
PDX 13-789	This paper	Duke University DNA Analysis Facility Human cell line authentication
Experimental Models: Organisms/Strains		
JAX NOD.CB17-PrkdcSCID-J mice	Duke University Rodent Genetic and Breeding Core	Stock No: 001303 RRID:IMSR_JAX:001303
Oligonucleotides		
siRNA/shRNA/RT-qPCR sequences see Table S1	This paper	N/A

(*Continued on next page*)

Continued

REAGENT or RESOURCE	SOURCE	IDENTIFIER
Recombinant DNA		
pLenti-EF-FH-TAZ S89A-ires-blast	(Yang et al., 2014b)	Addgene plasmid #52084
pLX304	(Yang et al., 2011)	Addgene plasmid #25890
pLX304-EMP1	(Yang et al., 2011)	DNASU# HsCD00442695
pcDNA3.1-hNOX4	(Serrander et al., 2007)	Addgene plasmid # 69352
Software and Algorithms		
GraphPad PRISM	GraphPad software	https://www.graphpad.com/scientific-software/prism/
TreeView	(Saldanha, 2004)	http://jtreeview.sourceforge.net
FlowJo software	FlowJo, LLC	RRID:SCR_008520

LEAD CONTACT AND MATERIALS AVAILABILITY

Further information and requests for resources and reagents should be directed to and will be fulfilled by the Lead Contact, Jen-Tsan Chi (jentsan.chi@duke.edu).

MATERIALS AVAILABILITY STATEMENT

This study did not generate new unique reagents.

EXPERIMENTAL MODEL AND SUBJECT DETAILS

Cell Culture Studies

RCC cell lines (RCC4 and 786O) were kind gifts from Dr. Denise Chan (Department of Radiation Oncology, University of California, San Francisco), which were further authenticated by DDC (DNA Diagnostics Center) Medical using the short tandem repeat method in November 2015. HEK293T and MDA-MB-231 were acquired from the Duke Cell Culture Facility. All cells are cultured in Dulbecco's Modified Eagle Medium (11995-DMEM, ThermoFisher Scientific) with 10% heat-inactivated Fetal Bovine Serum (HyClone^{TM} FBS, GE Healthcare Life Sciences #SH30070.03HI) in a humidified incubator at 37°C and 5% CO_2. Transfections were performed according to the manufacturer's instructions with TransIT-LT1 transfection reagent (Mirus Bio) or RNAiMax transfection reagent (ThermoFisher Scientific).

Stable cell lines were generated with the pLKO.1 puro control vector or shTAZ constructs purchased from the Duke Functional Genomics Shared Resource. The virus was generated by transfecting HEK293T cells with a 1: 0.1: 1 ratio of psPAX2: pMD2.G: pLKO.1 with Mirus transit reagent. Media was changed after 16 h and the virus was collected 40 h and 64 h after transfection. The virus soup was further centrifuge and went through the filter to remove cell debris. Stable cell lines were generated by adding 1ml virus soup to a 10 cm dish of parental cells with a final concentration of 8 μg/ml polybrene and selected by 0.5 μg/μl puromycin.

250 786O stable control (pLKO.1) or TAZ knockdown (shTAZ) cells were resuspended in 5μl medium and further mixed with 55 μl growth factor reduced Matrigel (Corning #356231) and then seeded in the center of 24 well plates. After the mixture became solid (37°C for 30 min), the 3D culture was kept in the puromycin-containing medium for 1 week. Later, the culture medium with or without 0.5μM erastin was changed every other day for 7-10 days; representative views from three independent experiments were photographed, and the colony sizes were measured.

Animal Models

All experiments were performed following Duke Institutional Animal Care and Use Committee approval in accordance with the institutional and national guidelines. Mice were housed with no more than 5 animals per cage and given free access to food and water. One million 786O cells with or without shTAZ were implanted subcutaneously into the healthy 8-week-old JAX NOD.CB17-PrkdcSCID-J mice; both male and female mice were used. Later, tumors were measured by caliper and the volumes were determined as (width^2 × length)/2. Once tumor volume reached 120 mm^3, mice were randomized into control or erastin treatment group. The vehicle (ORA-plus) or erastin (0.1ml of 4mg/ml erastin) was administrated by oral gavage twice daily for 20 days.

Patient-Derived Xenograft

Renal cell carcinoma (RCC) tissue sample (13-789) was collected under a Duke IRB-approved protocol (Pro000022289) and all participants provided written informed consent to participate in the study. The patient-derived xenograft (PDX) model of 13-789 was then generated as described previously (Kim et al., 2012; Uronis et al., 2012), and the *in vivo* PDX generation was performed in accordance

with the animal guidelines and with the approval of the Institutional Animal Care and Use Committee (IACUC) at the Duke University Medical Center. Briefly, to generate PDXs, the tissue sample was washed in phosphate-buffered saline (PBS), dissected into small pieces (< 2 mm), and injected into the flanks of 8-10-week-old JAX NOD.CB17-PrkdcSCID-J mice obtained from the Duke University Rodent Genetic and Breeding Core. The matched PDX cell line (13-789) was then generated from the PDX as follows. Once the PDX tumors reached a size of >1000 mm^3, tumors were harvested, homogenized, and grown in 10 cm^2 tissue culture-treated dishes in cell culture media (DMEM media, 10% fetal bovine serum (FBS), 10 U/ml penicillin and streptomycin) at 37°C and 5% CO_2. Clonal populations of each cell line were then obtained by isolating a single clone using trypsinization of the clone sealed off from the dish by an O ring. Finally, the 13-789 cell line was authenticated using the Duke University DNA Analysis Facility Human cell line authentication (CLA) service by analyzing DNA samples from each individual cell line for polymorphic short tandem repeat (STR) markers using the GenePrint 10 kit from Promega (Madison, WI, USA).

METHOD DETAILS

Determine of cell viability, cell death, and glutathione level

Unless otherwise stated in the figure legend, the genetic experiments were conducted when the cell density is around 50%–80% confluency after the cells were seeding and transfected with siRNAs for 2 days. The cells are further treated with erastin for additional 24 h-72 h. Cell viability was evaluated using crystal violet staining or the CellTiterGlo luminescent cell viability assay kit (Promega) which determined cellular viability using ATP levels; cytotoxicity was determined by SYTOX Green staining (Thermo) or CytoTox-Fluor assay (Promega); and the level of reduced glutathione (GSH) was detected by GSH/GSSG-Glo assay (Promega) by subtracting the oxidized glutathione (GSSG) level from the total (GSH plus GSSG) glutathione according to the manufacturer's instructions.

Western blot analysis

For immunoblotting, cells were washed with ice-cold phosphate-buffered saline (PBS), lysed in RIPA buffer (Sigma), supplemented with protease inhibitor (Roche) and PhosSTOP phosphatase inhibitor cocktail (Roche). Proteins were quantified by BCA protein assay (ThermoFisher Scientific). Equal amounts of proteins were resolved by sodium dodecyl sulfate–polyacrylamide gel electrophoresis (SDS-PAGE) and transferred to the polyvinylidene difluoride (PVDF) membrane (Millipore). The membranes were blocked with 5% non-fat milk or BSA and then probed with indicated antibodies following by HRP-conjugated secondary antibodies. The immunosignals were achieved by the Amersham ECL prime western blotting detection reagent (GE Healthcare Life Sciences RPN2232) and detected by a Bio-Rad ChemiDoc™ Imaging System.

RNA isolation and quantitative real-time PCR

Total RNAs of culture cells were extracted by using the RNeasy Mini Kit (QIAGEN #74104) with DNase I treatment (QIAGEN #79254) and the cDNAs were synthesized from 1 μg of the RNA template using SuperScript™ II Reverse Transcriptase (ThermoFisher Scientific #18064) with random hexamers following protocols from the manufactures. The levels of gene expression were measured by quantitative PCR (qPCR) with Power SYBR Green PCR Mix (Applied Biosystems, ThermoFisher Scientific).

Microarray

RCC4 cells exposed to knockdown control, siNT, or knockdown TAZ, siTAZ for two days and then treated with or without 1 μM erastin for 7 h in biological triplicates. RNAs were extracted by RNeasy Kit (QIAGEN), labeled, and hybridized to Affymetrix U133A 2.0 arrays. The intensities of Affymetrix probes were normalized by Robust Multi-array Average (RMA) method and zero transformation ($\Delta\log_2$) against the control group, siNT (DMSO) as previously performed (Keenan et al., 2015; Tang et al., 2017). Then, the probe sets that varied by $2^{0.8}$-fold in at least two samples were selected for hierarchical clustering. The microarray data have been deposited into NCBI GEO with accession number: GSE121689.

Immunofluorescence staining

Cells were cultured on chamber slide (ThermoFisher Scientific #177437) to appropriate density. Cells were fixed with 4% formaldehyde for 10 min and then washed three times with PBS. After blocking in 5% BSA and permeabilized with 0.1% Saponin for 1 h, slides were incubated with the TAZ antibody (BD Biosciences #560235) 1:100 diluted in 1% BSA with 0.1% Saponin overnight. After washing with PBS, slides were incubated with Alexa Fluor 488-conjugated secondary antibodies (1:200 dilution, ThermoFisher Scientific #A11001) and Alexa Fluor 568-conjugated phalloidin (ThermoFisher Scientific #A12380) for 1 h. The slides were then washed and mounted with SlowFade Glod antifade mountant with DAPI ((ThermoFisher Scientific #S36938). Images were acquired using a Leica TCS SP8 confocal microscope equipped with a 40X objective.

ChIP analysis

ChIP-qPCR experiment was carried out according to the Myers Lab ChIP-seq protocol (Johnson et al., 2007). Briefly, RCC4 cells were incubated in cross-linking solution (1% formaldehyde) at room temperature for 10 min and then added 0.125M final concentration of glycine to stop cross-linking. The cells were then washed with cold PBS and suspended in Farnham lysis buffer (5mM PIPES pH8.0, 85mM KCl and 0.5% NP-40) with freshly added protease inhibitor. The lysate was subsequently passed through a 20-gauge

needle 20 times to breaks cells while keeping intact nuclei. After centrifugation, the pellet was resuspended with RIPA buffer with freshly added protease inhibitor. Chromatin fragmentation was performed by sonication using the Bioruptor (Diagenode) high speed for 30 min (30 s ON, 30 s OFF). Proteins were immunoprecipitated in PBS/BSA buffer using TAZ antibody (Cell signaling #70148) or control antibody, rabbit IgG (Cell signaling #2729) which have been conjugated to Dynabeads™ protein G magnetic beads (Thermo Fisher Scientific #10004D) at 4°C for 2 hr. The antibody-chromatin complexes were washed with LiCl wash buffer for 5 times and then washed with TE buffer. The crosslinking was reversed by incubation with elution buffer (1%SDS, 0.1M $NaHCO_3$) at 65°C overnight followed by incubated with RNase A and proteinase K. DNA was recovered by using QIAquick PCR purification kit (QIAGEN #28104). Precipitated DNA was analyzed by qPCR using primers targeting TEAD-binding sites found in CTGF (Stein et al., 2015) and EMP1 promoter regions as well as negative control chromatin 14 (Stein et al., 2015). Primer sequences are listed below.

Lipid ROS assay using flow cytometry

Lipid ROS levels were determined using 10 μM of C11-BODIPY dye (D3861, ThermoFisher Scientific) with the positive control, cumene hydroperoxide, according to the manufacturer's instructions. Cells were seeded and treated with siRNAs in six-well plates for two days, then the culture medium was replaced with 1μM erastin treatment for overnight. The next day, the medium was replaced with 10 μM C11-BODIPY-containing medium for 1 h. Later, the cells were harvested by trypsin and washed three times with ice-cold PBS followed by re-suspending in PBS plus 1% BSA. The amount of ROS within cells was examined by flow cytometry analysis (FACSCanto™ II, BD Biosciences).

QUANTIFICATION AND STATISTICAL ANALYSIS

Graphs were drawn and statistics were analyzed by using GraphPad Prism 8 Software (GraphPad La Jolla, CA). Data were analyzed using two-tailed unpaired Student's t test or ANOVA (one-way or two-way) and expressed as mean ± SEM *p values* less than 0.05 were considered significant (* < 0.05; ** < 0.01; *** < 0.001). The exact values of "n" used are described in the corresponding figure legends. Unless otherwise stated in the figure legend, n refers to the number of biological replicates and includes either number of mice or replicates of cell studies.

DATA AND CODE AVAILABILITY

The microarray data of TAZ knockdown have been deposited into NCBI GEO with accession number: GSE121689. The siRNA screen of cystine deprivation has not been deposited in a public repository because the manuscript in preparation, but are available from the corresponding author on request.

Cell Reports, Volume *28*

Supplemental Information

The Hippo Pathway Effector TAZ Regulates Ferroptosis in Renal Cell Carcinoma

Wen-Hsuan Yang, Chien-Kuang Cornelia Ding, Tianai Sun, Gabrielle Rupprecht, Chao-Chieh Lin, David Hsu, and Jen-Tsan Chi

Figure S1 (related to Figure 1)

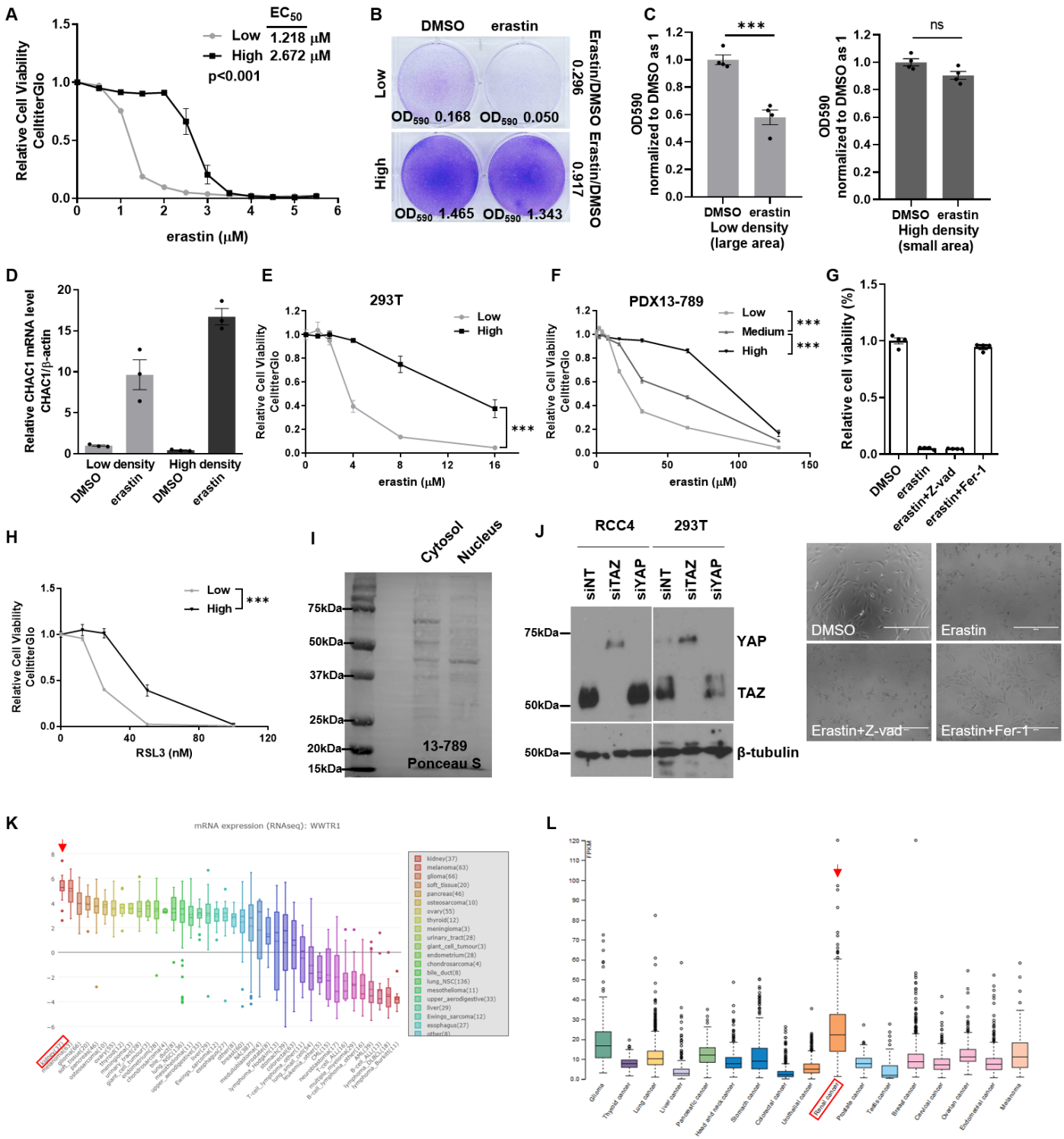

Figure S1 (related to Figure 1)

(A) Cell viability assay by CelltiterGlo after RCC4 cells, grown at low or high cell densities, were treated with indicated concentrations of erastin for 3 days to determine the EC_{50} at low and high cell density. (n=3; mean ± SEM; two-way ANOVA). (B) Crystal violet staining of RCC4, cultured at low or high densities, were treated with vehicle or 1μM erastin. Raw data and the ratios between the erastin/DMSO of OD590 are shown. (C) Quantitative analysis of crystal violet stain of RCC4 cells at low and high cell density (related to Figure 1D) after normalization to DMSO group using a microplate reading at OD 590 nm (n=4; mean ± SEM; Student's *t*-test). (D) *CHAC1* mRNA expression levels in the erastin-treated RCC4 grown at low or high density were determined by RT-qPCR. Data represented are mean±SEM, n=3 after normalized to the DMSO control of low density. (E) The cell viability of 293T cells was determined by CelltiterGlo when grown at low vs. high (2500/10,000 cells per 96 well) cell densities treated with indicated concentrations of erastin. (The data shown are from one representative experiment with three biological replicates, and the data were reproduced from two independent experiments; mean ± SEM; two-way ANOVA; ***$p < 0.001$). (F) The cell viability of PDX 13-789 cells was determined by CelltiterGlo when grown at low, medium or high (2250/4500/9000 cells per 96 well) densities and treated with indicated concentrations of erastin for 72 h. (n=3; mean ± SEM; two-way ANOVA; ***$p < 0.001$). (G) Cell viability of RCC4 was determined by CelltiterGlo and bright field images when RCC4 cells were treated with 1μM erastin, 20μM Z-VAD-FMK (Z-vad), or 1μM ferrostatin-1 (Fer-1). Scale bar, 200 μm. (H) Cell viability was determined by CelltiterGlo after RCC4 cells grown at low/high cell densities, and treated with indicated concentrations of RSL3 (n=3; mean ± SEM; two-way ANOVA; ***$p < 0.001$). (I) The Ponceau S staining blot of RCC PDX cytosolic and nucleic extractions as a loading control. (J) Western blot measuring YAP and TAZ protein levels in RCC4 and 293T cell lines treated with siRNA non-targeting (siNT) control or siRNAs targeting TAZ (siTAZ) or YAP (siYAP). (K) TAZ mRNA (*WWTR1*) expression in various indicated cell lines from the CCLE dataset (https://portals.broadinstitute.org/ccle) with the kidney cell lines indicated by the arrow. (L) TAZ mRNA (*WWTR1*) expression in TCGA dataset with the renal tumors indicated by the arrow. Data is retrieved from The Human Protein Atlas (https://www.proteinatlas.org/).

Figure S2 (related to Figure 2)

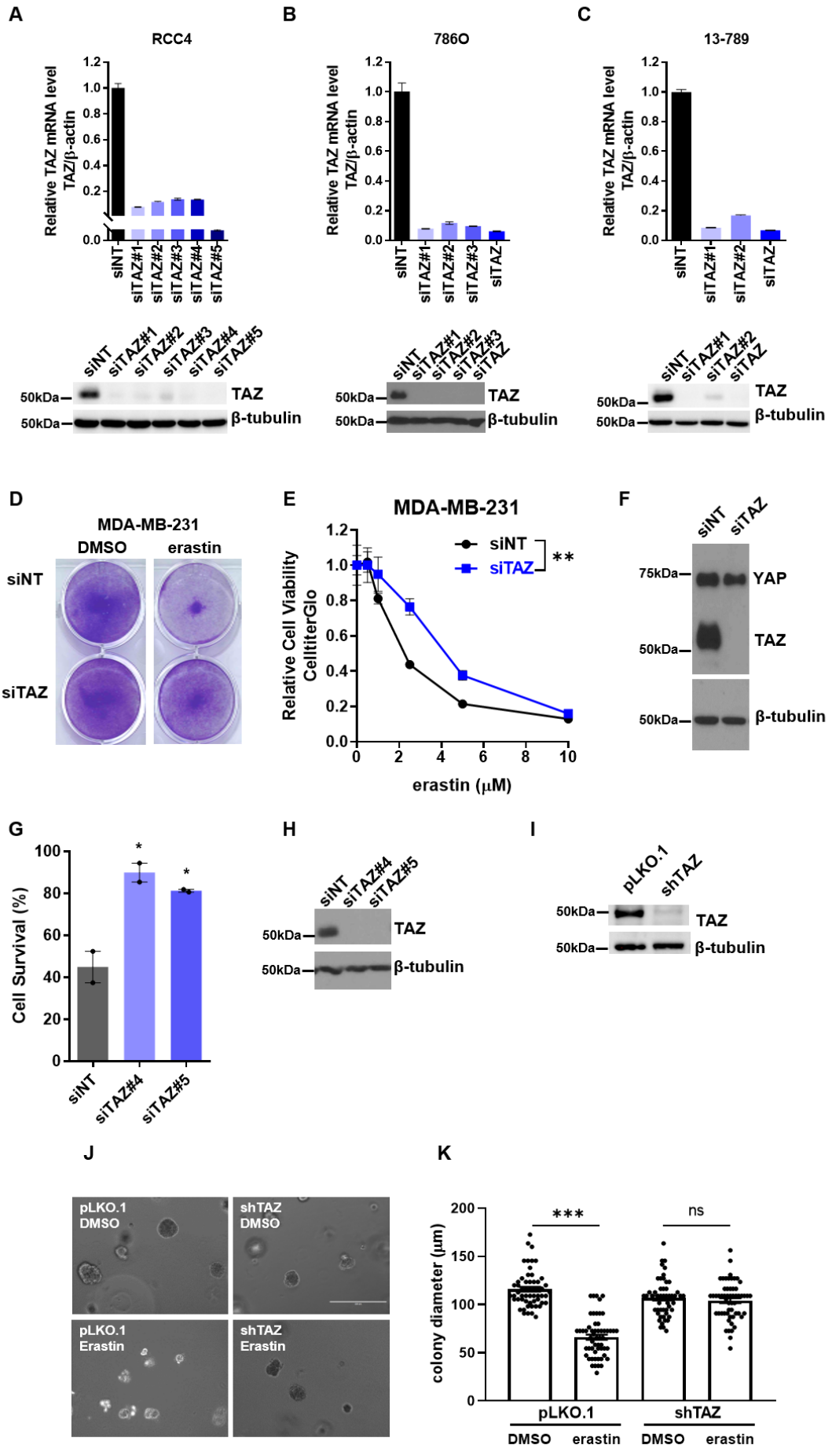

Figure S2 (related to Figure 2)

(A-C) The knockdown efficiency of various TAZ-targeting siRNAs was confirmed by western blot and RT-qPCR in RCC4 cells (A), 786O cells (B), or RCC PDX 13-789 cells (C). (D-F) MDA-MB-231 cells were treated with siRNA control (siNT) or siRNA targeting TAZ (siTAZ) for two days. The transfected cells were treated by indicated concentrations of erastin for 24 h and cell viability was determined by crystal violet staining (D) or CelltiterGlo (n=3; two-way ANOVA; $^{**}p < 0.01$) (E). The knockdown efficiency and specificity of TAZ were confirmed by western blots (F). (G-H) MDA-MB-231 cells were treated with two additional TAZ-targeting siRNAs (confirmed by western blots (H)) for two days following by treatment of 2.5μM erastin for 24 hours. The viability was determined by CelltiterGlo. Data are represented as mean±SEM and by comparing to the DMSO controls of each group (n=2; one-way ANOVA; $^{*}p < 0.05$). (I) Western blot confirmed the knockdown efficiency of shRNA targeting TAZ in 786O cells used for xenografts (related to Figure 2J-K) and 3D spheres in Matrigel (related to Figure S2J-K). (J-K) 3D Matrigel culture of 786O cells transduced with either control (pLKO.1) or TAZ-targeting shRNA. The formed spheres were treated with DMSO or 0.5μM erastin for 7-10 days before the measurement of colony diameters. (n=56 each group; two-way ANOVA; $^{***}p < 0.001$, ns: not significant).

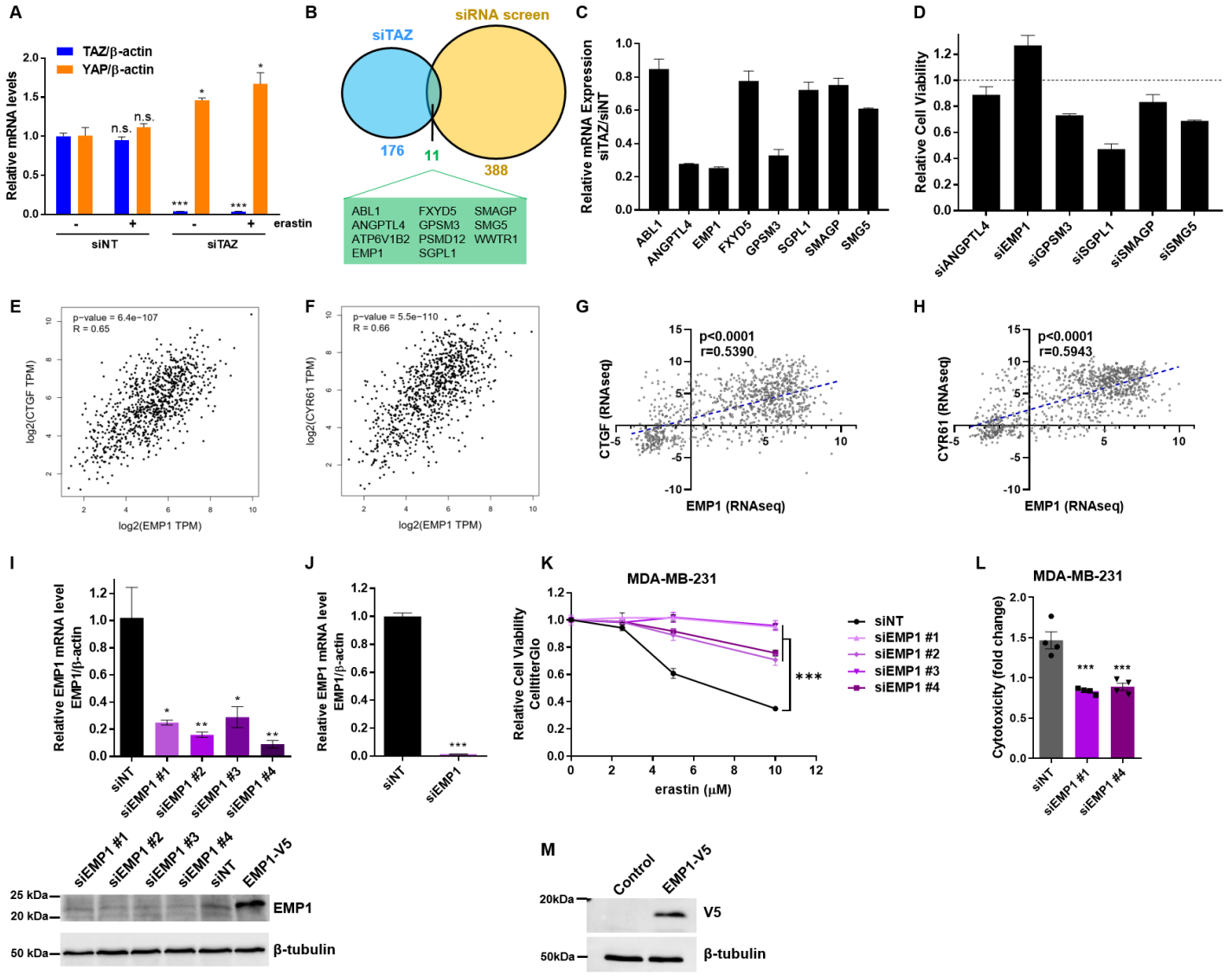

Figure S3 (related to Figure 3)

(A) RT-qPCR validates the knockdown efficiency of siTAZ for the RNA samples used for microarray analysis. Data represented are mean±SEM, n=3 after normalized to the DMSO controls. (B) Venn diagram showing genes that are downregulated upon siTAZ (176 genes) and siRNA screen of genes that are resistant to cystine deprivation (388 genes). (C) The knockdown efficiencies of siRNAs targeting indicated candidate genes were validated by RT-qPCR in RCC4 cells. (D) Functional assays of candidate genes that can affect ferroptosis. RCC4 cells were transfected with indicated siRNA(s) and treated with erastin. The cell viability data were determined by CelltiterGlo and showed as the ratio of siRNA(s) to siNT control after normalization of its own 2μM erastin to DMSO, that is, $siRNA^{erastin/DMSO}/siNT^{erastin/DMSO}$. (E-F) The correlation between the expression of indicated genes in the TCGA kidney cancer datasets. Data is retrieved from GEPIA (http://gepia.cancer-pku.cn/) with Spearman correlation analysis. TPM: Transcripts Per Kilobase Million. (G-H) The correlation between the expression of EMP1 and indicated canonical TAZ target genes in the CCLE dataset. Data were downloaded and re-graphed by GraphPad PRISM with Spearman correlation analysis. (I) The knockdown of various EMP1-targeting siRNAs was validated by RT-qPCR and western blots in RCC4 cells, related to Figure 3C. (J) The knockdown of EMP1 was validated by RT-qPCR in 786O cells, related to Figure 3D. (K) Cell viability was determined by CelltiterGlo after MDA-MB-231 cells were treated with siNT or individual siRNAs targeting EMP1 (#1 to #4) for two days following by treating with indicated concentrations of erastin. Data are represented as mean±SEM, n=3 by normalized to the DMSO controls of each group (n=3; two-way ANOVA; ***$p < 0.001$). (L) Cytotoxicity was determined by CytoTox-Fluor assay after treatment of 8μM erastin in the MDA-MB-231 cells with or without EMP1 knockdown (n=4; one-way ANOVA; ***$p < 0.001$). (M) Validation of EMP1 overexpression by V5 tag antibody.

Figure S4 (related to Figure 4)

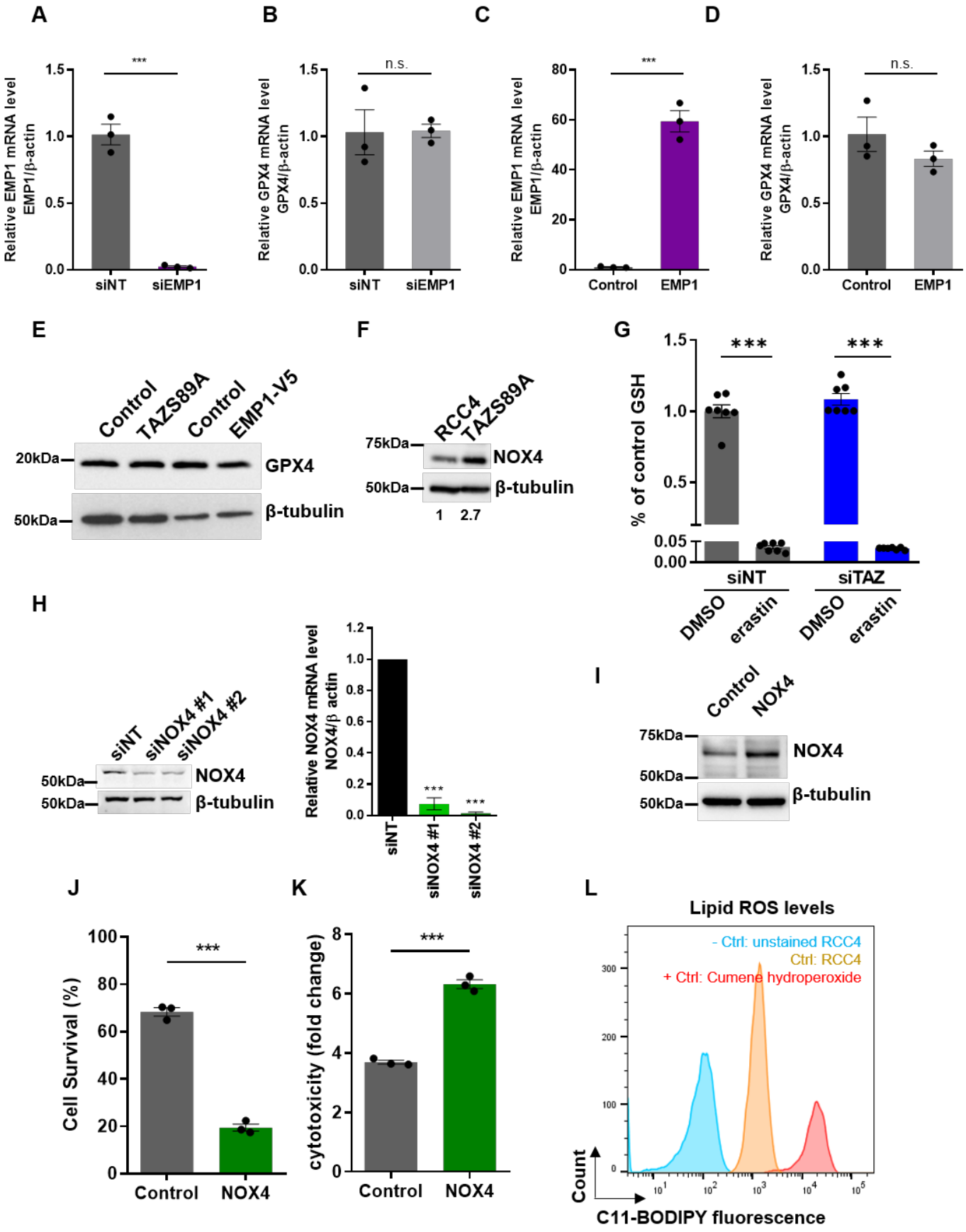

Figure S4 (related to Figure 4)

(A-D) RT-qPCR of EMP1 (A, C) or GPX4 (B, D) mRNA level upon siRNA-mediated knockdown of EMP1 (A, B) or EMP1 overexpression (C, D) (n=3; mean ± SEM; Student's *t*-test; ***p < 0.001; ns: not significant). (E) Western blot of GPX4 protein level in RCC4 upon the overexpression of TAZS89A or EMP1. (F) Western blot of NOX4 protein level in RCC4 upon the overexpression of TAZS89A. (G) The GSH (glutathione) levels in RCC4 were determined after TAZ knockdown followed by 1μM erastin treatment for 1 day and normalized to the siNT DMSO (n=7; mean ± SEM; two-way ANOVA; ***p < 0.001). (H) The knockdown of NOX4 by siRNAs in RCC4 was validated by RT-qPCR and western blot. (I-K) NOX4 overexpression (I) sensitized RCC4 cells to erastin treatment (4 μM) as determined by CelltiterGlo (J) or CytoTox-Fluor assay (K); n=3; mean ± SEM; Student's *t*-test; ***p < 0.001. (L) The negative (unstained) and positive controls (cumene hydroperoxide) for C11-BODIPY flow cytometry.

Table S1 (related to STAR Methods)

siRNA(s)	**Company/Cat No.**
siNT	Qiagen/SI03650318
siTAZ	Dharmacon/M-016083-00-0002
siYAP	Dharmacon/M-012200-00-0005
siEMP1	Dharmacon/M-010507-00-0005
siNOX4	Dharmacon/M-010194-00-0005
siANGPTL4	Dharmacon/M-007807-02-0005
siGPSM3	Dharmacon/M-013906-00-0005
siSMAGP	Dharmacon/M-015427-01-0005
siSMG5	Dharmacon/M-014023-00-0005
siTAZ #1	AGACATGAGATCCATCACTAA
siTAZ #2	ACAGTAGTACCAAATGCTTTA
siTAZ #3	CTGCGTTCTTGTGACAGATTA
siTAZ #4	GACAUGAGAUCCAUCACUA
siTAZ #5	GGACAAACACCCAUGAACA
siEMP1 #1	CAUCUACACUAGUCAUUAU
siEMP1 #2	ATCGCTACTGTTATTATGCTA
siEMP1 #3	ACCGTATTTCAGCCATGATAA
siEMP1 #4	CAUCAUCGGCGUUCUCUAU
siNOX4 #1	AACCAGGAGATTGTTGGATAA
siNOX4 #2	CAGCATCTGTTCTTAACCTCA
primers for RT-qPCR	**Sequences**
β actin-F'	GGGGTGTTGAAGGTCTCAAA
β actin-R'	GGCATCCTCACCCTGAAGTA
TAZ-F'	TGCTACAGTGTCCCCACAAC
TAZ-R'	GAAACGGGTCTGTTGGGGAT
YAP-F'	CAACTCCAACCAGCAGCAAC
YAP-R'	TTGGTAACTGGCTACGCAGG
EMP1-F'	GTGCTGGCTGTGCATTCTTG
EMP1-R'	CCGTGGTGATACTGCGTTCC
NOX4-F'	CAGATGTTGGGGCTAGGATTG
NOX4-R'	GAGTGTTCGGCACATGGGTA
GPX4-F'	GAGGCAAGACCGAAGTAAACTAC
GPX4-R'	CCGAACTGGTTACACGGGAA
primers for ChIP	**Sequences**
CTGF-F'	GCCAATGAGCTGAATGGAGT
CTGF-R'	CAATCCGGTGTGAGTTGATG
EMP1-F'	TTTGGTGAGGAGGAATGGGC
EMP1-R'	CAGTCAAGAGTGGCTGGGAG
Ch14-F'	GTGGGCCTTTGGAATATCCT
Ch14-R'	GACCTTGGCTGTGTTGTCCT
shRNA	**Duke Functional Genomics Shared Resource**
shTAZ	CCGGGCCCTTTCTAACCTGGCTGTACTCGAGTACAGCCAGGTTAGAAAGGGCTTTTT